AIAA JOURNAL
Vol. 33, No. 4, April 1995

Prediction of Two-Dimensional Momentumless Wake by k-ε-γ Model

Jong Woo Ahn*
Korea Research Institute of Ships and Ocean Engineering, Taejon 305-606, Republic of Korea
and
Hyung Jin Sung†
Korea Advanced Institute of Science and Technology, Taejon 305-701, Republic of Korea

The k-ε-γ model performance is extended to resolve the jet/wake anomaly, which is encountered in calculating free shear flows by the standard k-ε model. In the k-ε-γ model, the relation between the rate of dissipation ε and the level of intermittency γ is well incorporated. The model is run to predict the two-dimensional momentumless wake where a jet and a wake coexist. The predictions of the k-ε-γ model are compared with those of the k-ε model as well as the experiment. It is shown that the model performance is generally satisfactory.

Introduction

IN the 1980–81 AFOSR-HTTM-Stanford Conference on Complex Turbulent Flows, the plane–wake/plane–jet anomaly was pointed out. This indicates the contradictory behavior of predicted results for plane far wake when the eddy viscosity k-ε model is used.[1] For example, when the model constants are adjusted to predict spreading rate of the plane jet correctly, the spreading rate of the plane wake is underpredicted by as much as 30% below the experimental values.[2] This implies that in the jet the calculated dissipation rate is lower than the experimental value, but the trend is reversed in the wake.[3] Such a discrepancy is thought to be a critical source of the anomaly, which suggests that there should be other physical mechanisms participating in the dissipation process. It is well known that, in computing turbulent free shear flows, the rate of dissipation at a point is closely related to the level of the intermittency.[4,5]

There have been a number of attempts to remedy this defect.[6–9] In particular, serious efforts have been made to reflect the effect of intermittency in developing computational intermittency models.[10–14] They suggested a new eddy viscosity relation, which was modified with an intermittency factor γ. Cho and Chung,[3] among others, recently proposed a k-ε-γ model, based on the conventional Reynolds-averaged moments, to incorporate the intermittency effect in the k-ε equations. The proposed k-ε-γ model successfully resolved the anomaly problem of various turbulent free shear flows, e.g., a plane jet, a round jet, a plane far wake, and a plane mixing layer.

In the present paper, the preceding k-ε-γ model is extended to consider the case where a jet and a wake coexist. As remarked earlier, the net momentum flux in the streamwise direction is negative in the wake and positive in the jet. If a jet and a wake are simultaneously present, this combined structure offers a significant flow setup for a test of the aforementioned anomaly. In particular, if the jet strength is adjusted to balance the wake drag, the net momentum deficit becomes zero; the downstream flow is known as a momentumless wake. A typical example can be found in the wake of a self-propelled body moving at constant velocity. However, the momentumless wake differs from the individual jet and wake flows because the production of turbulence decays rapidly, causing a loss of balance between production and dissipation. The present endeavor of predicting the momentumless wake with the k-ε-γ model is not only important for the model performance, but it is also of interest in acquiring an understanding of the characteristics of the momentumless wake.

A survey of literature on momentumless wakes reveals that many theoretical and experimental studies have been made.[15–17] An overview was given in Park[18] and Cimbala and Park.[19] It is noticed that most of the previous studies have reported mainly on axisymmetric momentumless wakes, and experimental studies of two-dimensional wakes with the addition of thrust are not numerous. Recently, Cimbala and Park performed a comprehensive experiment of a two-dimensional momentumless wake ($Re = 5.4 \times 10^3$) to provide a complete set of accurate flow data. The emphasis was focused on measurements of the mean profiles and turbulence intensities. Smoke-wire flow visualizations at several downstream locations in the wake were made to document the scales of turbulent structure. A brief review of numerical studies on momentumless wakes by using turbulence models was also contained in their papers.[18,19]

In this study, we applied the k-ε-γ model to predict a two-dimensional momentumless wake, which encompasses the aforementioned typical jet/wake anomaly. As mentioned earlier, Cho and Chung applied the k-ε-γ model to test for several elemental free shear flows. However, they computed only the similarity profiles of thin boundary-layer-type flow at high Reynolds number. On the contrary, in the present treatise, we deal with the whole flowfield around a two-dimensional momentumless wake. Attention is directed to the model performance. The predicted results are compared against the output of the standard k-ε model as well as the published experimental data.[19,20] The model validations are extended to the cases of an asymmetric jet and a dual jet in the momentumless wakes to scrutinize the effect of initial conditions on two-dimensional momentumless far wakes. It is shown that the two-dimensional momentumless wakes are simulated successfully with the present k-ε-γ model. Furthermore, based on the computational results, the detailed turbulent structure of the momentumless wake is analyzed satisfactorily.

Governing Equations and Numerical Procedure

Governing Equations

The continuity equation and the Reynolds time-averaged Navier–Stokes equations for an incompressible, steady flow are written in a Cartesian tensor form as follows:

$$\frac{\partial}{\partial x_i}(U_i) = 0 \tag{1}$$

$$\frac{\partial}{\partial x_i}(U_i U_j) = -\frac{1}{\rho}\frac{\partial p}{\partial x_i} + \frac{\partial}{\partial x_j}\left[(\nu + \nu_t)\left(\frac{\partial U_i}{\partial x_j} + \frac{\partial U_j}{\partial x_i}\right) - \frac{2}{3}k\delta_{ij}\right] \tag{2}$$

Received July 21, 1994; revision received Nov. 10, 1994; accepted for publication Nov. 14, 1994.

*Senior Research Scientist, KIMM, P.O. Box 1, Daeduck Science Town.
†Professor, Department of Mechanical Engineering, 373-1, Kusong-dong, Yusong-ku.

where ρ is the density of fluid, U the mean velocity, p the mean pressure, and k the turbulent kinetic energy, respectively.

The transport equations for turbulence closure are the equations for the turbulent kinetic energy k, the rate of kinetic energy dissipation ε, and the intermittency factor γ.[3] The turbulent kinetic energy equation is as follows:

$$\frac{\partial}{\partial x_i}(U_i k) = \frac{\partial}{\partial x_i}\left(\frac{\nu_t}{\sigma_k}\frac{\partial k}{\partial x_i}\right) + P - \varepsilon \tag{3}$$

where P represents the production of k due to the shear strain and the normal strain. These are given by

$$P = -\overline{u_i u_j}\frac{\partial U_i}{\partial x_j} = \nu_t\left(\frac{\partial U}{\partial y} + \frac{\partial V}{\partial x}\right)^2 - \left(\overline{u^2} - \overline{v^2}\right)\frac{\partial U}{\partial x} \tag{4}$$

Following Hanjalic and Launder,[21] the normal stress difference is approximated as a constant fraction of the turbulent kinetic energy:

$$\left(\overline{u^2} - \overline{v^2}\right) = C_{uv}k \tag{5}$$

As pointed out in Cho and Chung,[3] the rate of dissipation at a point is closely associated with the level of intermittency. When the intermittency γ is low, the small-scale eddies are relatively inactive and the turbulent kinetic energy is slowly dissipated. However, when the intermittency γ is high, the energy dissipation becomes large by the presence of the fine-scale eddy motions embedded in the energetic large straining eddies in the interactive shear layer between the turbulent and irrotational zones. In an effort to incorporate this effect of intermittency on the rate of dissipation, the conventional equation of the rate of dissipation is modified. A convenient measure to represent the additive source (or sink) of the intermittency γ at a certain point, under consideration due to the entrainment process, is the concept of intermittency invariant Γ. The modified equation of the rate of dissipation is written as follows:

$$U_i\frac{\partial \varepsilon}{\partial x_i} = \frac{\partial}{\partial x_i}\left[\frac{\nu_t}{\sigma_\varepsilon}\frac{\partial \varepsilon}{\partial x_i}\right] + \frac{\varepsilon^2}{k}\left[C_{\varepsilon_1}\frac{P}{\varepsilon} - C_{\varepsilon_2} + C_{\varepsilon_4}\Gamma\right] \tag{6}$$

where

$$\Gamma \equiv \frac{k^{2.5}}{\varepsilon^2}\frac{U_i}{(U_l U_l)^{0.5}}\frac{\partial U_i}{\partial x_j}\frac{\partial \gamma}{\partial x_j} \tag{7}$$

Here, the vortex stretching invariant term χ, used in the ε equation of Cho and Chung,[3] which was originally proposed by Pope,[4] is dropped in Eq. (6) since χ vanishes in two-dimensional flow. It is noted that when the frame of reference is moving at the constant velocity U_r, then the velocity U in Eq. (7) should be replaced by $U_r - U$ to secure the Galilian invariance of the scalar Γ.

The governing equation for the intermittency factor has the form

$$U_j\frac{\partial \gamma}{\partial x_j} = D_g + S_g \tag{8}$$

where

$$D_g = \frac{\partial}{\partial x_j}\left[(1-\gamma)\frac{\nu_t}{\sigma_g}\frac{\partial \gamma}{\partial x_j}\right] \tag{9}$$

$$S_g = C_{g1}\gamma(1-\gamma)\frac{P}{k} + C_{g2}\frac{k^2}{\varepsilon}\frac{\partial \gamma}{\partial x_j}\frac{\partial \gamma}{\partial x_j} - C_{g3}\gamma(1-\gamma)\frac{\varepsilon}{k}\Gamma \tag{10}$$

In the preceding equations, D_g is a conventional diffusion model, and S_g represents the conversion rate of the irrotational fluid into the turbulent one. The terms on the right-hand side of Eq. (10) denote the generation of γ, the increase of γ by the spatial inhomogeneity, and the interaction between the mean velocity gradient and the intermittency fluid, in sequence, respectively. Details regarding the modeling of each term can be found in Cho and Chung.[3]

Finally, the eddy viscosity is expressed as a function of k, ε, and γ:

$$\nu_t = C_\mu\left[1 + C_{\mu g}\frac{k^3}{\varepsilon^2}\gamma^{-m}(1-\gamma)\frac{\partial \gamma}{\partial x_k}\frac{\partial \gamma}{\partial x_k}\right]\frac{k^2}{\varepsilon} = C'_\mu\frac{k^2}{\varepsilon} \tag{11}$$

It is noted that the preceding eddy viscosity model reduces to the usual form, when γ is set 1.0 in the fully turbulent zone. The values of model constants adopted in the present k-ε-γ model are the same as those values of Cho and Chung[3]; $C_\mu = 0.09$, $C_{\mu g} = 0.10$, $m = 3.0$, $C_{uv} = 0.33$, $\sigma_k = 1.0$, $\sigma_\varepsilon = 1.0$, $\sigma_g = 1.0$, $C_{\varepsilon 1} = 1.44$, $C_{\varepsilon 2} = 1.92$, $C_{\varepsilon 4} = 0.1$, $C_{g1} = 1.6$, $C_{g2} = 0.15$, and $C_{g3} = 0.16$.

Numerical Method and Boundary Conditions

The differential equations governing the mean and turbulent flowfields are solved numerically by the well-established finite volume method.[22–24] In this study, a nonorthogonal curvilinear coordinate system is adopted, and the grid system is nonstaggered. The momentum interpolation method proposed by Rhie and Chow[22] is used to avoid the problem of the pressure–velocity decoupling encountered at the nonstaggered grid system. The coupling between pressure and velocity is achieved by the SIMPLEC predictor–corrector algorithm of Van Doormal and Raithby,[25] which is an improved version of the SIMPLE algorithm. The convection terms in U, V, k, ε, and γ equations are discretized by using the hybrid linear/parabolic approximation (HLPA) scheme,[26] which satisfies the convection boundedness criterion and is of second-order accuracy. Each discretized governing equation is solved iteratively by the strongly implicit procedure (SIP) method,[27] until a converged solution is obtained. Convergence is declared if the absolute sum of nondimensional residuals of each governing equation throughout the computation domain is less than 10^{-4}. All of the calculations were implemented on a Cray Y-MP supercomputer, and a typical CPU time was approximately 3 h for one set of calculations.

The schematic diagram around a two-dimensional momentumless wake model is shown in Fig. 1. At the upstream, the freestream velocity U_∞ and the freestream turbulence level of 0.1% are given from available experimental data.[18–20] An important point in applying the k-ε-γ model is the inlet condition of γ. In the present computation, the upstream boundary value of γ is specified to be a very small one, i.e., $\gamma = 0.001$. This is justified in that the upstream is assumed to be an irrotational zone. The Neumann boundary conditions for all variables are applied at the outlet. No-slip and impermeable conditions are imposed on the model surface.

The calculations of the near-wall region are carried out by bridging the viscosity-affected near-wall layers by means of wall functions. Since the k-ε-γ model is not directly applicable in the viscosity-affected region, the first grid point away from the wall is placed outside the viscous sublayer. Actually, the y_p^+ values at the first grid points are within 13–21 in the present computations. The boundary value of the intermittency is set to be unity, because the first grid points from the wall are located in the fully turbulent region. The jet velocity U_j and the turbulent

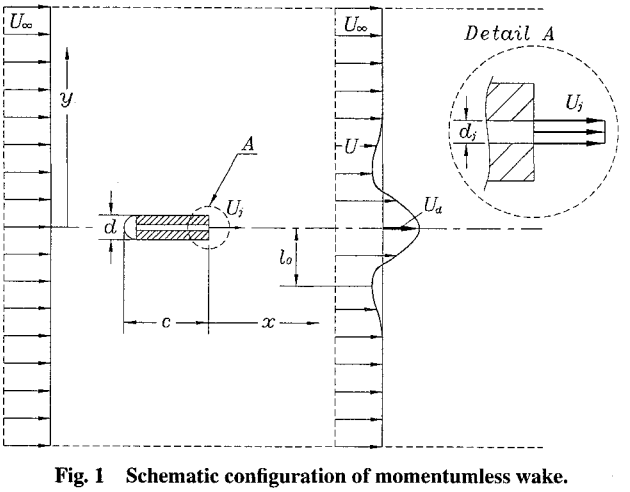

Fig. 1 Schematic configuration of momentumless wake.

kinetic energy k_j at the jet exit are given from the experimental conditions.[18–20] The turbulent kinetic energy k_j is set to be 0.5% of the mean kinetic energy U_j^2. The dissipation rate ε_j is not usually available from the experiment; therefore, a simple algebraic fomulation is used, $\varepsilon_j = k_j^{3/2}/l_j$, where l_j is a turbulent length scale. This length scale is approximated as $l_j = 0.3d_j$.[28,29] The sensitivity of the solutions to the jet exit conditions has been checked by changing the length scale l_j. A careful test indicates that the predicted results are not sensitive to their initial conditions, as long as the momentumless state is maintained in the flowfield.

Computational Results and Discussion

The main objective of the present study is to remedy the jet/wake anomaly by using the k-ε-γ model. The momentumless wake, where a jet and a wake coexist, is the target flow. The k-ε-γ model[3] adopted here is known to describe adequately the interaction between the mean shear and intermittency fields. The experiments of Park,[18] Cimbala and Park,[19] and Park and Cimbala[20] for a two-dimensional momentumless wake flow are employed to validate the present model predictions.

A schematic sketch of the flow configuration is shown in Fig. 1, together with the coordinate (x, y) and the corresponding velocity components. The centerline velocity difference U_d is defined as the absolute difference between the freestream velocity U_∞ and the mean centerline velocity. The length scale l_o represents the distance from the centerline at which the velocity U reaches the minimum. The chord length c of the model is $4.66d$, whereas the jet injection slit d_j at the back is $0.168d$. The Reynolds number based on the model diameter d is 5.4×10^3.

Before proceeding further, it is important to ascertain the grid dependence of the computational results. The typical grid system is illustrated in Fig. 2, which shows the detailed grid around the central single-jet model. The minimum grid spacing near the model wall is $0.038d$, and the lateral boundaries for the computation are located at $7.85d$ from the model. The inlet and outlet boundaries are located $10.4d$ upstream and $80.0d$ downstream, respectively. The computations are carried out with the two different grid systems, i.e., (160×111) nodes and (240×161) nodes. The comparison for the mean velocity and turbulent kinetic energy profiles at different locations ($x/d = 15$ and 45) is presented in Fig. 3, which demonstrates the grid convergence of the solutions. These results give credence to the reliability and accuracy of the present calculations.

Now, the mean velocity profiles behind the momentumless wake model are plotted at five different stations ($x/d = 5$–45) in Fig. 4. The computational results by employing the present k-ε-γ model as well as the standard k-ε model are presented together with the experimental data of Park[18] and Cimbala and Park.[19] It is encouraging that the computed mean velocity distributions by the k-ε-γ model are in good agreement with the experiment in the entire flowfield. Only in the near-wake region ($x/d = 5$), some discrepancy is seen. As shown in Fig. 4, the mean shear near the centerline decays rapidly along the distance downstream. For example, the mean velocity profile at $x/d = 45$ is shown to be almost flat. In contrast, the predicted results by the standard k-ε model represent a slow recovery of the mean velocity defect and they produce narrow spreading rates. These phenomena may be attributed to the typical jet/wake anomaly, for which the standard k-ε model is not well suited.

It is worthwhile discussing the improvement of the k-ε-γ model performance from the viewpoint of intermittency γ. As emphasized earlier, both a jet and a wake are simultaneously present in the momentumless wake. Consider two different cases separately. In the case of a jet, the inner product between the entrainment vector $-\nabla(P/\rho)$ and the intermittency gradient vector $\nabla\gamma$ is positive, and the pressure field drives more irrotational fluid towards the more turbulent region, i.e., the inward movement of the more irrotational fluid. This gives rise to an increase of the dissipation ε, which is reflected effectively in the γ equation. Similarly, a reverse situation is encountered in a wake. Here, the inner product becomes negative, and ε is reduced owing to the outward movement of the more turbulent fluid. For these reasonings, the predicted results by the k-ε-γ model are improved considerably. Details concerning the relation between the rate of dissipation and the level of intermittency are described in Cho and Chung.[3] The change of ε by intermittency can be adjusted by the intermittency interaction invariant Γ in Eq. (7). Consequently, the k-ε-γ model enables more physically realistic modulations of ε, depending upon the relative direction of the entrainment process. The argument of the momentum transfer in the momentumless wake is properly reflected.

Comparisons are extended to the distributions of turbulent kinetic energy k/U_∞^2 and the corresponding Reynolds stress $-\overline{uv}/U_\infty^2$, as displayed in Figs. 5 and 6. The computed results of k/U_∞^2 by the two models agree reasonably well with the experiment. However, in the near-wake region, both models are seen to overpredict the level of turbulence. This discrepancy is thought to be attributable to the fact that the present two models did not include the effect of anisotropy but considered only the total sum, i.e., $k = 0.5(\overline{u^2} + \overline{v^2} + \overline{w^2})$. As demonstrated in Park[18] and Cimbala and Park,[19] the structure of anisotropy in the near-wake region was clearly shown; the peak axial turbulence intensity $\overline{u^2}$ is about 5–10% greater than the transverse intensity $\overline{v^2}$ or lateral intensity $\overline{w^2}$ near the centerline ($\overline{u^2} > \overline{v^2} > \overline{w^2}$).

The predicted Reynolds stress profiles are shown together with the experimental data in Fig. 6. The results computed by the k-ε-γ model are satisfactory, even in the near-wake region. A closer inspection of the distributions near the center region reveals that the aforestated important role of γ acts very reasonably; Γ is negative in the wake and positive in the jet. Owing to the multiple inflection points in the mean velocity profile (Fig. 4), the negative values of the Reynolds stress profile are clearly displayed. As stressed in Park,[18] and Cimbala and Park,[19] the negative profile is a unique feature of the momentumless wake. The negative portion of the Reynolds stress profile of the momentumless wake is formed due to

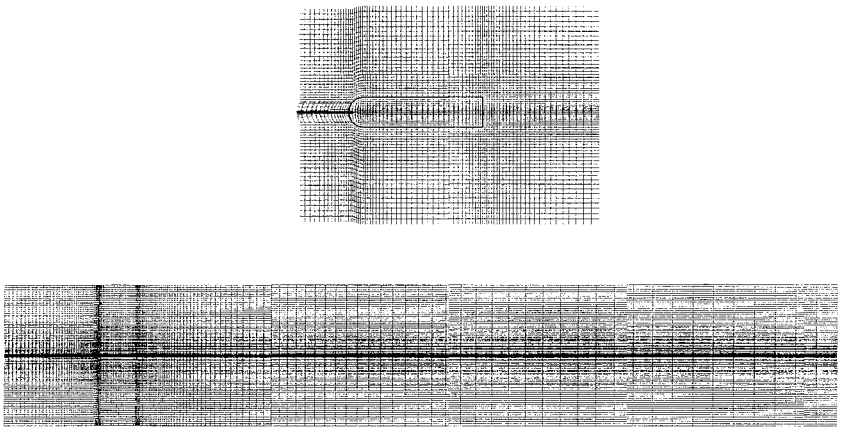

Fig. 2 Grid system around the momentumless wake model.

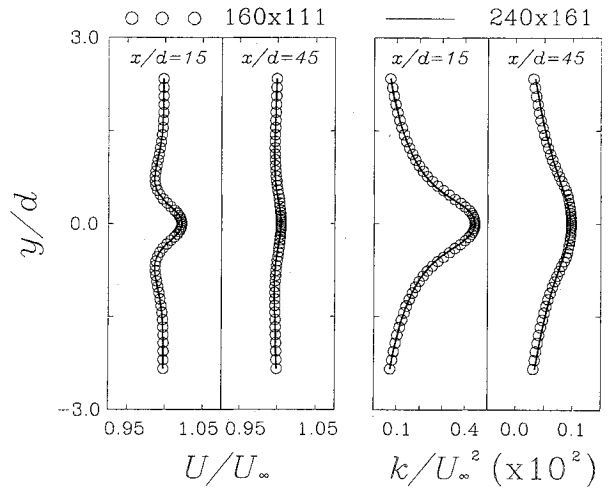

Fig. 3 Grid dependence evaluation of the computed results for 160 × 111 and 240 × 161.

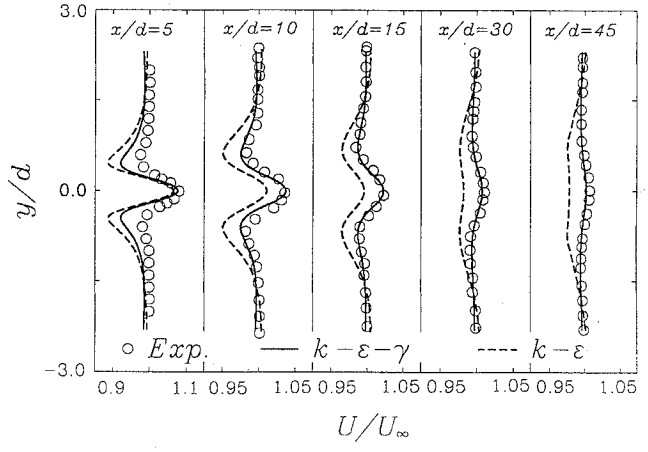

Fig. 4 Comparison of the predicted U/U_∞ with the experiment.

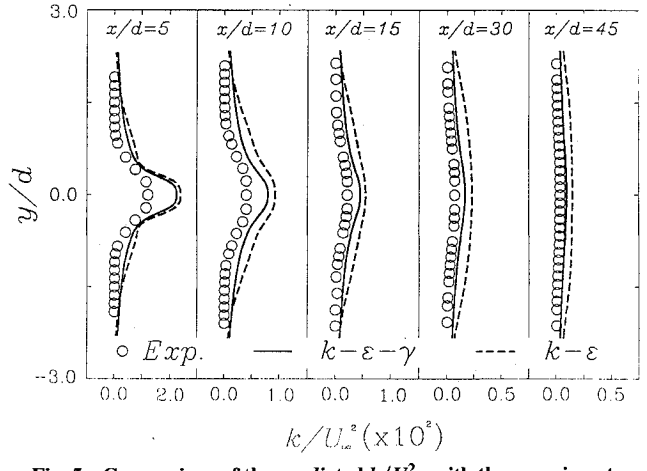

Fig. 5 Comparison of the predicted k/U_∞^2 with the experiment.

the additional momentum flux injected into the wake field. The normalized Reynolds stress profiles $\overline{uv}/\overline{uv}_{\max}$ vs y/l_0 for $x/d = 5$–45, which are not shown here, indicate that the Reynolds stresses are zero approximately at $y/l_0 \simeq 0.96$–1.0 in the present computation, whereas $y/l_0 \simeq 0.96$–1.05 in the experiment.[18,19] These excellent agreements reinforce the capability of the k-ε-γ model for predicting the momentumless wake flows. It is noted here that the zero Reynolds stress at $y/l_0 \simeq 0.96$–1.0 implies the zero mean shear in Fig. 4, which occurs quite close to the y/l_0 position of the secondary extrema in the mean velocity profiles ($y/l_0 \sim 1.0$).

Further evidence of the present model performance is seen in the comparison of the decay of centerline mean velocity defect and

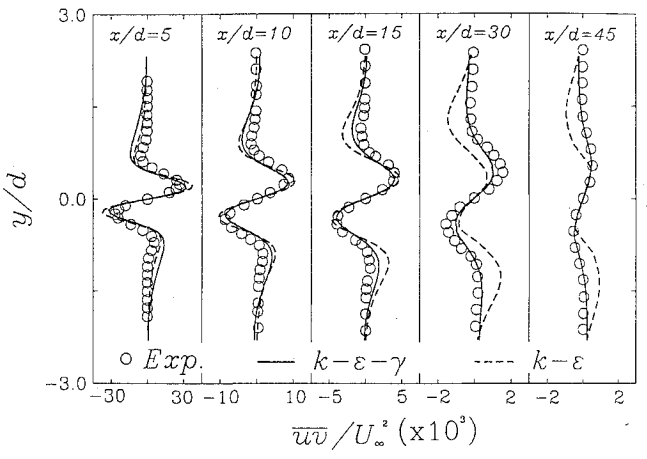

Fig. 6 Comparison of the predicted $\overline{uv}/U_\infty^2$ with the experiment.

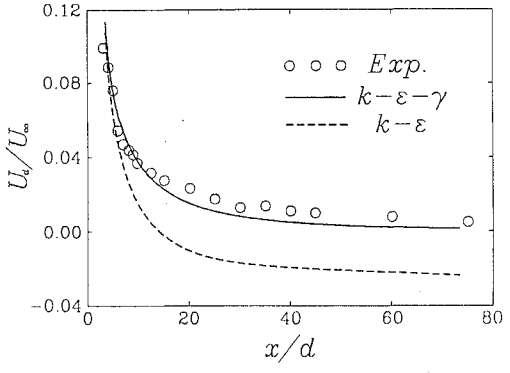

Fig. 7 Comparison of the predicted U_d/U_∞ with the experiment.

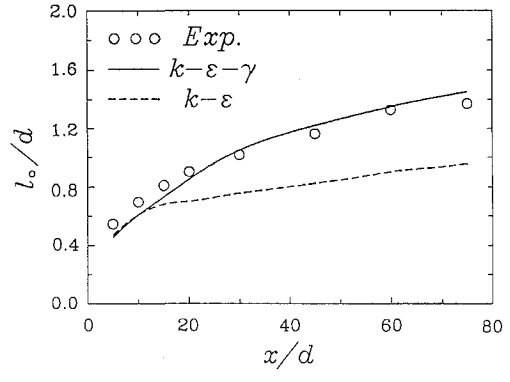

Fig. 8 Comparison of the predicted l_0/d with the experiment.

the spreading rate of the momentumless wake width with the experimental results. As in Figs. 7 and 8, the present computational results are in good agreement with the experiment. It is known that the momentumless wake decays rapidly compared with the elemental free shear flows, e.g., pure wake, weak wake, and weak jet.[18,19] Furthermore, as can be seen in Fig. 7, the prediction by the standard k-ε model intensifies the decay rate increasingly, even yielding negative values of U_d/U_∞ beyond the downstream ($x/d \geq 15$). This inadequate prediction is caused mainly by the current turbulence models, which were adjusted to the plane-jet flow predictions (jet/wake anomaly). Accordingly, the prediction by the k-ε model for the spreading rate of wake width also exhibits too narrow spreading rates along the downstream (Fig. 8). The improvement by the k-ε-γ model is clearly seen in Fig. 8.

The decay rate of the maximum Reynolds shear stress $\overline{uv}_{\max}/U_\infty^2$ is plotted in Fig. 9. The decay rate predicted by the k-ε-γ model is the same as the decay rate of the experiment,[18,19] which follows as $x^{-1.84}$. However, the prediction by the k-ε model deviates from the experimental data in the downstream beyond $x/d \simeq 30$. The decay

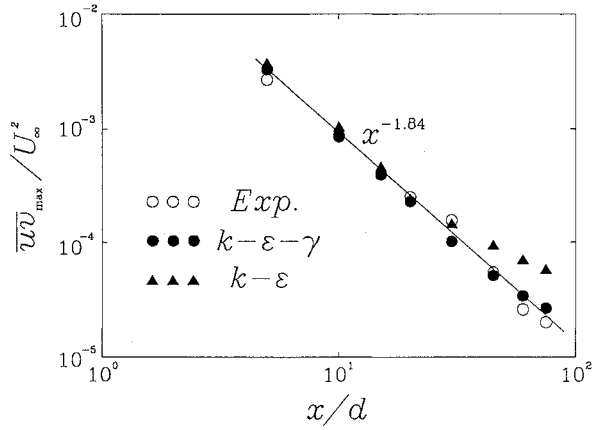

Fig. 9 Comparison of the predicted $\overline{uv}_{max}/U_\infty^2$ with the experiment.

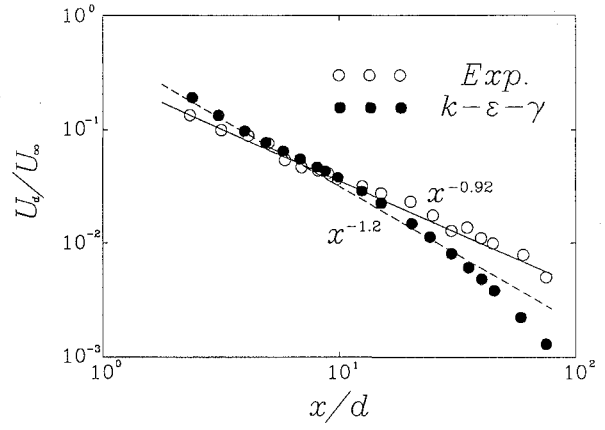

Fig. 10 Comparison of the predicted U_d/U_∞ with the experiment.

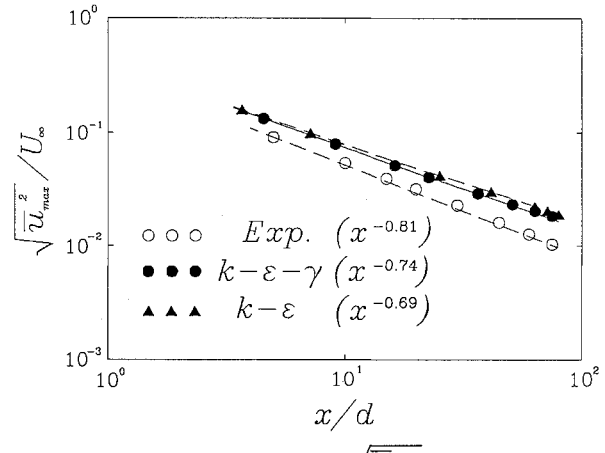

Fig. 11 Comparison of the predicted $\sqrt{\overline{u^2}_{max}}/U_\infty$ with the experiment.

of U_d (Fig. 7) is replotted on a log-log scale in Fig. 10. Contrary to the prior agreement in Fig. 7, a small deviation is observed in the far downstream, where the predicted decay rate ($U_d \sim x^{-1.2}$) by the k-ε-γ model is faster than that of the experiment. The experimental decay rate follows $U_d \sim x^{-0.92}$, which turns out to be exactly the same as the half of the decay rate of the preceding maximum Reynolds shear stress $\overline{uv}_{max} \sim x^{-1.84}$.

The decay rate of the maximum axial turbulence intensity $\sqrt{\overline{u^2}_{max}}/U_\infty$ is illustrated in Fig. 11. For the three cases, i.e., the experiment, the predictions by the k-ε-γ model, those and by the k-ε model, the decay laws follow $\sqrt{\overline{u^2}_{max}} \sim x^{-0.81}, x^{-0.74}$, and $x^{-0.69}$, respectively. Although the k-ε-γ model prediction is not entirely consistent with the experiment, it is in better agreement with the experiment than that of the k-ε model. As compared with the previous figures (Figs. 9 and 10), it is revealed that the decay rate of $\sqrt{\overline{u^2}_{max}}/U_\infty$ is much slower than those of U_d/U_∞ and $\overline{uv}_{max}/U_\infty^2$. Nevertheless, it is still faster than those of elementary free shear flows,[15,16] e.g., a pure wake ($x^{-0.5}$) and a plane jet ($x^{-0.5}$). This suggests that the present two-dimensional momentumless wake returns faster towards isotropic turbulence than other flows, at least beyond some distance.

Most elementary free shear flows are known to be asymptotically self-preserving. This implies that the production and its rate of dissipation of turbulent energy are in a local equilibrium state and the behavior far downstream becomes independent of the initial conditions. However, in the present analysis of momentumless wake flow, it is shown that the momentumless wake is different from other elementary free shear flows. Since momentumless wakes are produced by injection of fluid from the rear of a model such that the thrust exactly cancels the drag, the momentumless far wake is affected significantly by the jet injection configurations of the model. As stated earlier, the decay rates of U_d, $\overline{uv}_{max}$, and $\overline{u^2}_{max}$ for the present momentumless wake are much faster than those of elementary free shear flows. Especially, $\overline{uv}_{max}$ decays very rapidly. There have been several attempts to study the effect of the initial conditions on axisymmetric momentumless wakes. Among others, Finson[16] showed the dependency on the initial conditions by using the second-order turbulence model. The experimental endeavors can be found in Park[18] and Park and Cimbala.[20]

To scrutinize the effect of initial conditions on two-dimensional momentumless far wakes, we calculated the cases of different geometries of jet injection in the momentumless wakes. Park[18] and Park and Cimbala[20] made an experiment about three types of jet injection model: 1) a central single-jet injection model, 2) an asymmetric single-jet injection model, and 3) a dual-jet injection model. The central single-jet injection model corresponds to the afore-mentioned two-dimensional momentumless wake (Cimbala and Park[19]). The dual-jet model was fabricated by modifying the rear part of the air channel of the basic model to produce two outer jets, which are located symmetrically near the edges of the model. The asymmetric single-jet model was constructed simply by covering one of the dual-jet slits with a thin tape. Details regarding the model configurations are found in Park[18] and Park and Cimbala.[20]

The mean velocity profiles behind the dual-jet injection and asymmetric single-jet injection models are presented in Fig. 12. As in the previous results (Fig. 4), the computed results show similar features to those of the central single-jet model. The predicted mean velocity distributions by the k-ε-γ model are also in better agreement with the experiment except the near-wake region ($x/d = 5$). The results by the standard k-ε model represent a very slow recovery of the mean velocity defect. As is evident in Fig. 12, the predicted mean velocity profiles for the preceding two cases of the k-ε model display significant deviations along the downstream. Moreover, the deviation becomes wider for the dual jet than for the asymmetric single jet. From these results, it is seen that the k-ε model is not suitable to describe the effect of the initial conditions on the evolution of momentumless wakes.

The decays of the centerline velocity difference U_d are plotted on a log-log scale in Fig. 13. For the central single-jet, the asymmetric single-jet, and the dual-jet momentumless wakes, the decay laws by the k-ε-γ model follow $U_d \sim x^{-1.20}$, $x^{-1.35}$, and $x^{-1.86}$, respectively, and those by the experiment follow $U_d \sim x^{-0.92}$, $x^{-1.24}$, and $x^{-2.02}$, respectively. The predictions are found to be qualitatively consistent with the experiment. As remarked earlier, U_d shows a significant dependence on the initial conditions. No universal decay law for U_d seems to exist numerically and experimentally. Among the three momentumless wakes, the dual-jet injection model decays most rapidly, and the asymmetric single jet, decays faster than the central single-jet case.

The spreading rates of wake width in terms of l_0 are presented in Fig. 14 for the two different initial conditions. In the case of the central single-jet injection model, the spreading rate is calculated from the data of Fig. 8. For the central single-jet, the asymmetric single-jet, and the dual-jet momentumless wakes, the spreading rates by

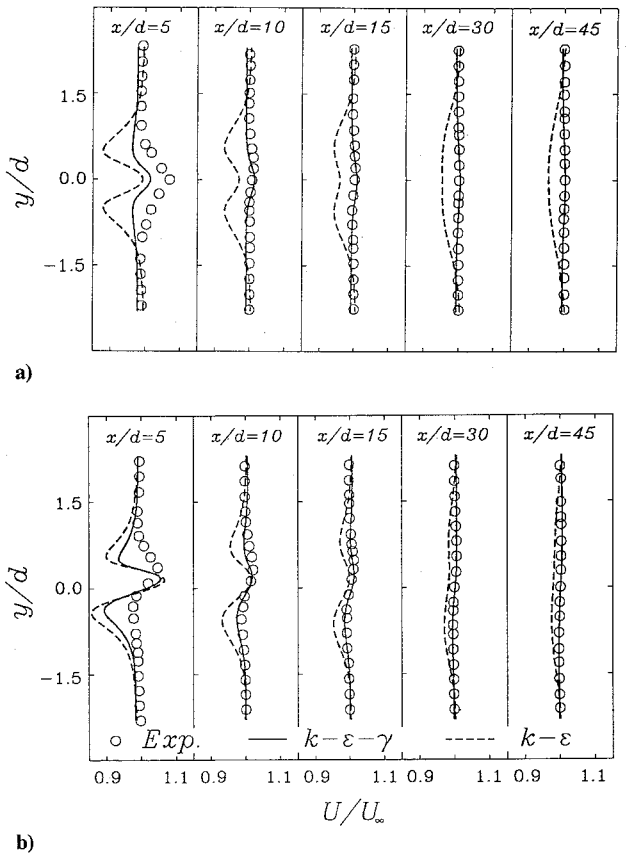

Fig. 12 Comparison of the predicted U/U_∞ with the experiment: a) dual-jet injection model and b) asymmetric single-jet injection model.

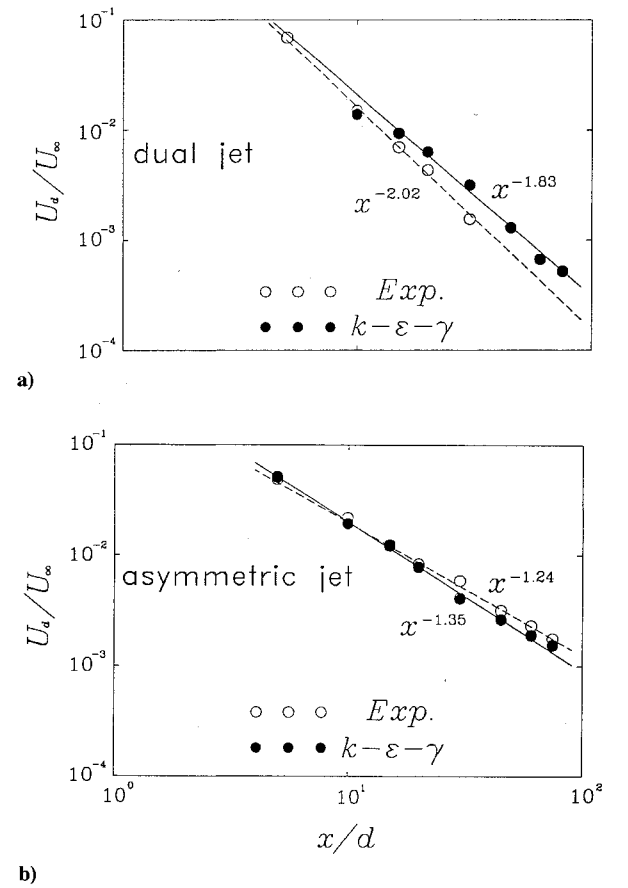

Fig. 13 Comparison of the predicted decay law of U_d/U_∞ with the experiment: a) dual-jet injection model and b) asymmetric single-jet injection model.

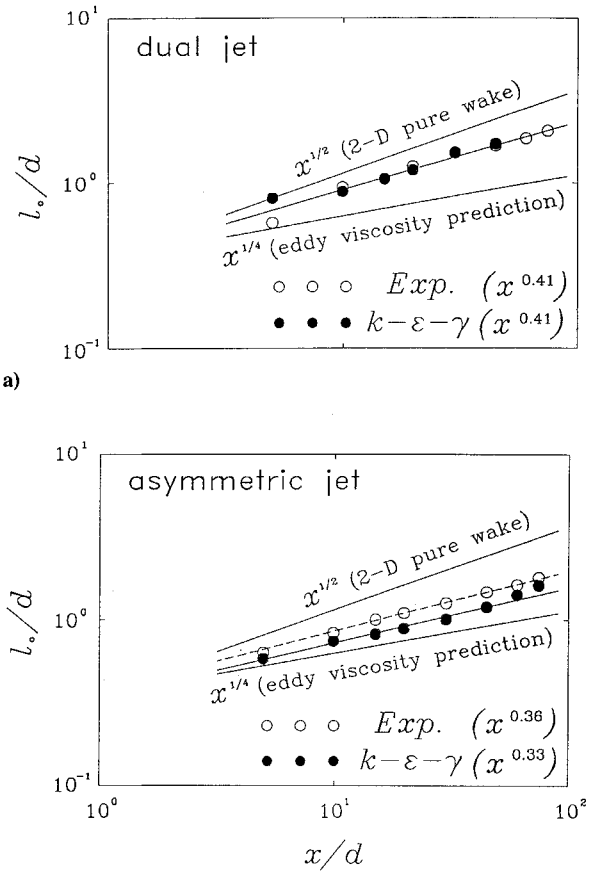

Fig. 14 Comparison of the predicted l_0/d with the experiment: a) dual-jet injection model and b) asymmetric single-jet injection model.

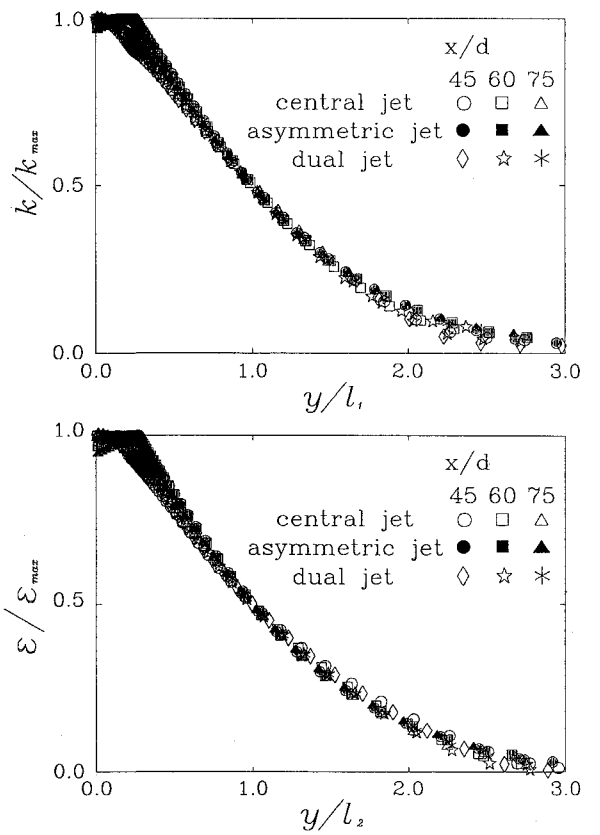

Fig. 15 Normalized profiles of k and ε for three momentumless far wakes with the k-ε-γ model.

the k-ε-γ model follow $l_0 \sim x^{0.35}$, $x^{0.33}$, and $x^{0.41}$, respectively, and those by the experiment follow $l_0 \sim x^{0.33}$, $x^{0.36}$, and $x^{0.41}$, respectively. As shown in Fig. 14, the central single-jet momentumless wake shows the slowest spreading rate, whereas the dual-jet momentumless wake shows the fastest spreading rate. For comparison, the constant-eddy-viscosity prediction of Tennekes and Lumley[30] ($x^{0.25}$) and the theoretically predicted value ($x^{0.50}$) for the pure wake are also drawn in Fig. 14. As is evident, the former underestimates the experimental and numerical results for two cases, and the latter overestimates. The spreading rates for all three cases fall between the eddy-viscosity prediction ($x^{0.25}$) and the analytical prediction ($x^{0.50}$). It is encouraging that the present k-ε-γ model predictions for the two cases are in broad agreement with the experimental data. The agreement is better in the dual-jet injection model than in the asymmetric single-jet injection model.

Finally, profiles of the turbulent kinetic energy k and its dissipation rate ε obtained by the three different injection configurations are plotted for $x/d = 45$, 60, and 75 in Fig. 15. Here, l_1 and l_2 represent the half-width of $k_{\max}$ and $\varepsilon_{\max}$, respectively. Contrary to the aforestated cases (U_d and l_0), the normalized profiles appear to be universal for all two-dimensional momentumless far wakes generated by different jet-injection models. Although U_d and l_0 show significant dependence on initial conditions, the present numerical simulations with the k-ε-γ model show that the rate of decay k is almost the same for all three models. Namely, for the central single-jet, the asymmetric single-jet, and the dual-jet momentumless far wakes, the decay laws by the k-ε-γ model follow $k \sim x^{-1.34}$, $x^{-1.33}$, and $x^{-1.31}$, respectively. These are closely consistent with the experimental findings.[20]

Conclusions

The two-dimensional momentumless wake, where a jet and a wake coexist, has been successfully resolved by employing the k-ε-γ model. Emphasis was placed on the remedy of the typical jet/wake anomaly in free shear flows. The k-ε-γ model was developed by introducing an intermittency interaction invariant Γ into the conventional k-ε model with an appropriate modification of the ε equation. It resolved physically realistic modulation of ε depending upon the relative direction of the entrainment process, and the argument of the momentum transfer in momentumless wake was properly reflected. The computed results for U and k by the k-ε-γ model were in good agreement with the experiment in the far wake regions, whereas those by the k-ε model showed a slower recovery of the mean velocity defect. Furthermore, the k-ε-γ model predicted the Reynolds shear stresses quite satisfactorily. The decay rates of U_d, l_0, $\overline{uv}_{\max}$, and $\overline{u^2}_{\max}$ in momentumless far wake regions were predicted by the k-ε-γ model, and they showed excellent agreement with the experiment. These decay rates of the momentumless wake were found to be faster than those of elementary free shear flows. The validation was extended to the flows of dual jet and of asymmetric jet to examine the effect of the initial conditions of the momentumless far wake. The computed results by the k-ε-γ model turned out to be adequate for the investigation of the effect of the initial conditions, whereas those by the k-ε model did not properly follow the mean velocity profiles of the experimental data. It was found that whereas U_d and l_0 show significant dependence on initial conditions, the rate of decay of k is almost the same for all three jet injection configurations.

Acknowledgment

Appreciation is extended to the referees, who provided detailed and helpful comments. These led to improvements in the revised paper.

References

[1]Kline, S. J., Cantwell, B., and Lilley, G. K. (eds.), "Comparison of Computation and Experiment," *Proceedings of the 1980–82 AFOSR-HTTM-Stanford Conference on Complex Turbulent Flows*, Stanford, 1981/82.

[2]Rodi, W., "A Review of Experimental Data of Uniform Density Free Turbulent Boundary Layers," *Studies in Convection*, edited by B. E. Launder, Vol. 1, Academic, New York, 1975, pp. 79–165.

[3]Cho, J. R., and Chung, M. K., "A Proposal of k-ε-γ Equation Turbulence Model," *Journal of Fluid Mechanics*, Vol. 237, 1992, pp. 301–322.

[4]Pope, S. B., "An Explanation of the Turbulent Round-Jet/Plane-Jet Anomaly," *AIAA Journal*, Vol. 16, 1978, pp. 279–281.

[5]Hanjalic, K., and Launder, B. E., "Sensitizing the Dissipation Equation to Irrotational Strains," *Journal of Fluids Engineering*, Vol. 102, 1980, pp. 34–40.

[6]Hanjalic, K., Launder, B. E., and Schiestel, R., "Multiple-Time-Scale Concepts in Turbulent Transport Modeling," *Turbulent Shear Flows 2*, edited by L. J. S. Bradbury, F. Durst, B. E. Launder, F. W. Schmidt, and J. H. Whitelaw, Springer–Verlag, New York, 1983, pp. 36–49.

[7]Launder, B. E., Morse, A. P., Rodi, W., and Spalding, D. B., "Prediction of Free Shear Flows—A Comparison of Six Turbulent Models," NASA SP 321, 1972.

[8]Mcguirk, J. J., and Rodi, W., "The Calculation of Three-Dimensional Turbulent Free Jet," *Turbulent Shear Flows 1*, edited by F. Durst, B. E. Launder, F. W. Schmidt, and J. H. Whitelaw, Springer–Verlag, New York, 1977, pp. 71–83.

[9]Morse, A. P., "Axisymmetric Turbulent Shear Flows with and without Swirl," Ph.D. Thesis, Univ. of London, London, 1977.

[10]Patel, V. C., and Scheuerer, G., "Calculation of Two-Dimensional Near and Far Wake," *AIAA Journal*, Vol. 20, 1981, pp. 900–907.

[11]Chevray, R. and Tutu, N. K., "Intermittency and Preferential Transport of Heat in a Round Jet," *Journal of Fluid Mechanics*, Vol. 88, 1977, pp. 136–160.

[12]Byggstoyl, S., and Kollmann, W., "A Closure Model for Conditional Stress Equations and Its Application to Turbulent Shear Flows," *Physics of Fluids*, Vol. 29, 1986, pp. 1430–1440.

[13]Cebeci, T., Clark, R. W., Chang, K.C., Halsey, N. D., and Lee, K., "Airfoils with Separation and the Resulting Wakes," *Journal of Fluid Mechanics*, Vol. 163, 1986, pp. 323–347.

[14]Haworth, D. C., and Pope, S. B., "A PDF Modeling Study of Self-Similar Turbulent Free Shear Flows," *Physics of Fluids*, Vol. 30, 1987, pp. 1026–1044.

[15]Naudascher, E., "Flow in the Wake of Self-Propelled Bodies and Related Sources of Turbulence," *Journal of Fluid Mechanics*, Vol. 22, Pt. 4, 1965, pp. 625–656.

[16]Finson, M. L., "Similarity Behavior of Momentumless Turbulent Wakes," *Journal of Fluid Mechanics*, Vol. 71, Pt. 3, 1975, pp. 465–479.

[17]Hassid, S., "Similarity and Decay Law of Momentumless Wakes," *Physics of Fluids*, Vol. 23, No. 2, 1980, pp. 404, 405.

[18]Park, W. J., "An Experimental Investigation of the Turbulent Structure in Two-Dimensional Momentumless Wakes," Ph.D. Thesis, Pennsylvania State Univ., University Park, PA, 1989.

[19]Cimbala, J. M., and Park, W. J., "An Experimental Investigation of the Turbulent Structure in a Two-Dimensional Momentumless Wake," *Journal of Fluid Mechanics*, Vol. 213, 1990, pp. 479–509.

[20]Park, W. J., and Cimbala, J. M., "The Effect of Jet Injection Geometry on Two-Dimensional Momentumless Wakes," *Journal of Fluid Mechanics*, Vol. 224, 1991, pp. 20–47.

[21]Hanjalic, K., and Launder, B. E., "A Reynolds Stress Model of Turbulence and Its Application to Thin Shear Flows," *Journal of Fluids Engineering*, Vol. 103, 1981, pp. 352–360.

[22]Rhie, C. M., and Chow, W. L., "A Numerical Study of the Turbulent Flow Past an Isolated Airfoil with Trailing-Edge Separation," *AIAA Journal*, Vol. 21, 1983, pp. 1525–1532.

[23]Peric, M., "A Finite Volume Method for the Prediction of Three-Dimensional Fluid Flow in Complex Ducts," Ph.D. Thesis, Univ. of London, London, Aug. 1985.

[24]Rodi, W., Majumdar, S., and Schonung, B., "Finite Volume Methods for Two-Dimensional Incompressible Flows with Complex Boundaries," *Computational Methods in Applied Mechanics and Engineering*, Vol. 75, 1989, pp. 369–392.

[25]Van Doormal, J. P., and Raithby, R. D., "Enhancement of the SIMPLE Method for Predicting Incompressible Fluid Flow," *Numerical Heat Transfer*, Vol. 7, 1984, pp. 147–163.

[26]Zhu, J., "A Low-Diffusive and Oscillation-Free Convection Scheme," *Communications in Applied Numerical Methods*, Vol. 7, 1991, pp. 225–232.

[27]Stone, H. L., "Iterative Solution of Implicit Approximations of Multidimensional Partial Differential Equations," *SIAM Journal of Numerical Analysis*, Vol. 3, No. 3, 1968, pp. 530–558.

[28]Leschziner, M. A., and Rodi, W., "Calculation of Annular and Twin Parallel Jets Using Various Discretization Schemes and Turbulence-Model Variations," *Journal of Fluid Mechanics*, Vol. 52, 1972, pp. 609–638.

[29]Zhang, X., "Interaction Between a Turbulent Boundary Layer and Elliptic and Rectangular Jets," *Engineering Turbulence Modeling and Experiments 2*, edited by W. Rodi and F. Martelli, 1993, pp. 251–260.

[30]Tennekes, H., and Lumley, J. L., *A First Course in Turbulence*, MIT Press, Cambridge, MA, 1972.